JACS
JOURNAL OF THE AMERICAN CHEMICAL SOCIETY

Communication

pubs.acs.org/JACS

Defect-Induced Band-Edge Reconstruction of a Bismuth-Halide Double Perovskite for Visible-Light Absorption

Adam H. Slavney,[†] Linn Leppert,[§,#] Davide Bartesaghi,[‡,⊥] Aryeh Gold-Parker,[†,▽] Michael F. Toney,[▽] Tom J. Savenije,[‡] Jeffrey B. Neaton,[*,§,#,∥] and Hemamala I. Karunadasa[*,†]

[†]Department of Chemistry, Stanford University, Stanford, California 94305, United States
[§]Molecular Foundry, Lawrence Berkeley National Laboratory, Berkeley, California 94720, United States
[#]Department of Physics, University of California Berkeley, Berkeley, California 94720, United States
[‡]Optoelectronic Materials Section, Department of Chemical Engineering, Delft University of Technology, 2628CD Delft, The Netherlands
[⊥]Materials Innovation Institute (M2i), 2628CD Delft, The Netherlands
[▽]Stanford Synchrotron Radiation Lightsource, SLAC National Accelerator Laboratory, Menlo Park, California 94025, United States
[∥]Kavli Energy NanoScience, Institute at Berkeley, Berkeley, California 94720, United States

Supporting Information

ABSTRACT: Halide double perovskites have recently been developed as less toxic analogs of the lead perovskite solar-cell absorbers $APbX_3$ (A = monovalent cation; X = Br or I). However, all known halide double perovskites have large bandgaps that afford weak visible-light absorption. The first halide double perovskite evaluated as an absorber, $Cs_2AgBiBr_6$ (**1**), has a bandgap of 1.95 eV. Here, we show that dilute alloying decreases **1**'s bandgap by ca. 0.5 eV. Importantly, time-resolved photoconductivity measurements reveal long-lived carriers with microsecond lifetimes in the alloyed material, which is very promising for photovoltaic applications. The alloyed perovskite described herein is the first double perovskite to show comparable bandgap energy and carrier lifetime to those of $(CH_3NH_3)PbI_3$. By describing how energy- and symmetry-matched impurity orbitals, at low concentrations, dramatically alter **1**'s band edges, we open a potential pathway for the large and diverse family of halide double perovskites to compete with $APbX_3$ absorbers.

Due to their rapid rise in power-conversion efficiencies, solar cells employing $APbI_3$ perovskite absorbers are now being considered for commercialization.[1] However, the toxicity of this water-soluble Pb^{2+} source remains a critical concern for the materials' large-scale manufacture and use.[2] The synthesis of a less toxic and stable analog that captures the remarkable photophysical properties of $APbI_3$ would constitute a critical advance in this field.[3] To mimic the electronic properties of $APbI_3$ we,[4] and others,[5] recently replaced Pb^{2+} with nontoxic, isoelectronic Bi^{3+}, by synthesizing the double perovskite $Cs_2AgBiBr_6$ (**1**) (Figure 1). Solid **1** is significantly more heat and moisture resistant than $(MA)PbI_3$ ($MA = CH_3NH_3^+$).[4] However, **1**'s indirect bandgap of 1.95 eV[4] provides inferior light absorption compared to the $APbI_3$ perovskites, which have direct gaps of ca. 1.6 eV. Here, we demonstrate how the photophysical properties of **1** can be made competitive with those of $(MA)PbI_3$ through dilute alloying.

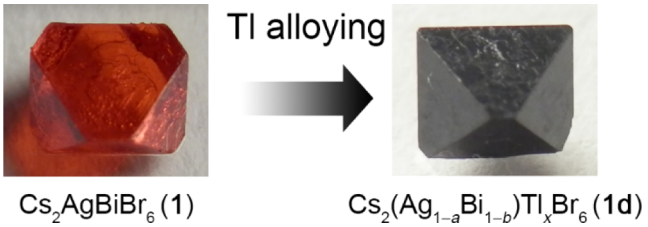

Figure 1. Photographs of $Cs_2AgBiBr_6$ (**1**) and $Cs_2(Ag_{1-a}Bi_{1-b})Tl_xBr_6$ (**1d**; $x = a + b = 0.075$) single crystals. Photograph of **1** reproduced from ref 4.

The $A_2BB'X_6$ double perovskites offer far greater diversity of B-site metals compared to ABX_3 perovskites. Although there has been much recent interest in halide double perovskites as solar-cell absorbers, these materials have so far displayed high bandgaps of 1.95−3.02 eV.[4−6] Lead's filled 6s orbitals at the valence-band maximum (VBM) and empty 6p orbitals at the conduction-band minimum (CBM) play an important role in $APbI_3$'s strong direct-gap absorption (Figure 2a).[7] The double perovskite $(MA)_2TlBiBr_6$ (**2**),[6c] where Pb^{2+} is replaced by isoelectronic Tl^+ and Bi^{3+}, has a similar orbital composition at its band edges (Figure 2b). Although both $(MA)PbI_3$ and **2** have direct transitions, inclusion of Ag s (Ag d) orbitals in **1** shifts the CBM (VBM) leading to an indirect gap.[5] We hypothesized that increasing $6s^2$ and $6p^0$ orbital character near **1**'s band edges may allow us to recover the direct gap of $APbI_3$. We therefore attempted to incorporate Tl^+ as a dilute impurity into **1**.

Solid **1** crystallizes as translucent orange truncated octahedra.[4] In contrast, adding TlBr to the crystallization solution affords opaque black octahedral crystals of the Tl-alloyed perovskite: **1d** (Figure 1). Using this method, the Tl content can be tuned across the series $Cs_2(Ag_{1-a}Bi_{1-b})Tl_xBr_6$ (**1d**, $0.003 < x = a + b <$

Received: February 15, 2017
Published: March 29, 2017

DOI: 10.1021/jacs.7b01629
J. Am. Chem. Soc. 2017, 139, 5015−5018

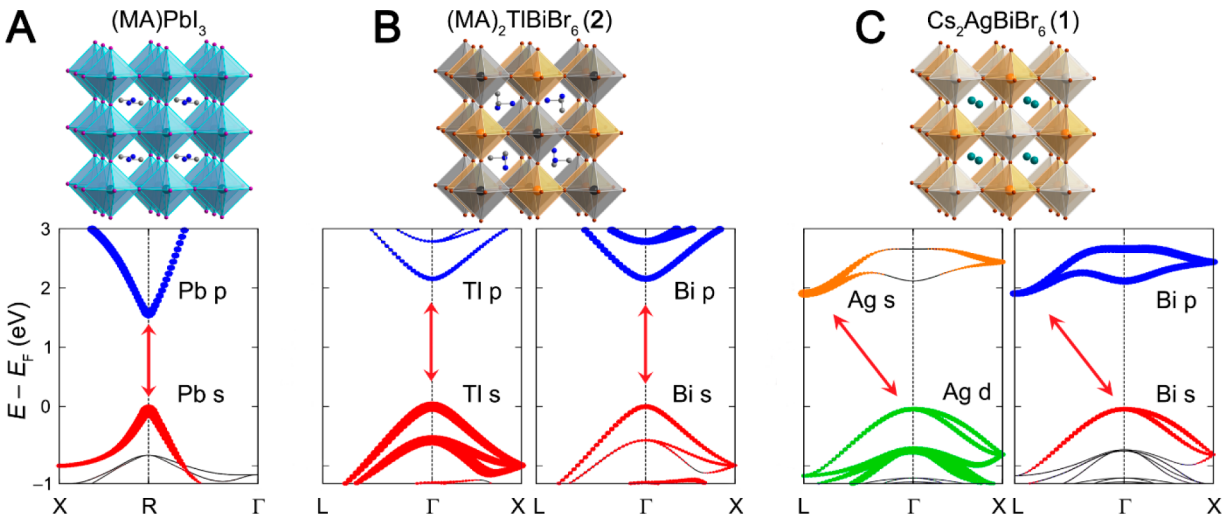

Figure 2. Crystal structures and band structures of (A) cubic $(MA)PbI_3$, (B) $(MA)_2TlBiBr_6$ (**2**), and (C) $Cs_2AgBiBr_6$ (**1**). The dominant metal orbital character of the bands is shown in color. Arrows show the direct (A and B) and indirect (C) bandgap transitions. In the primitive unit cell of **1**, the VBM appears at X, however, in the conventional setting shown here the VBM is at Γ due to band folding (see Supporting Information). Hydrogens and disordered atoms are omitted for clarity.

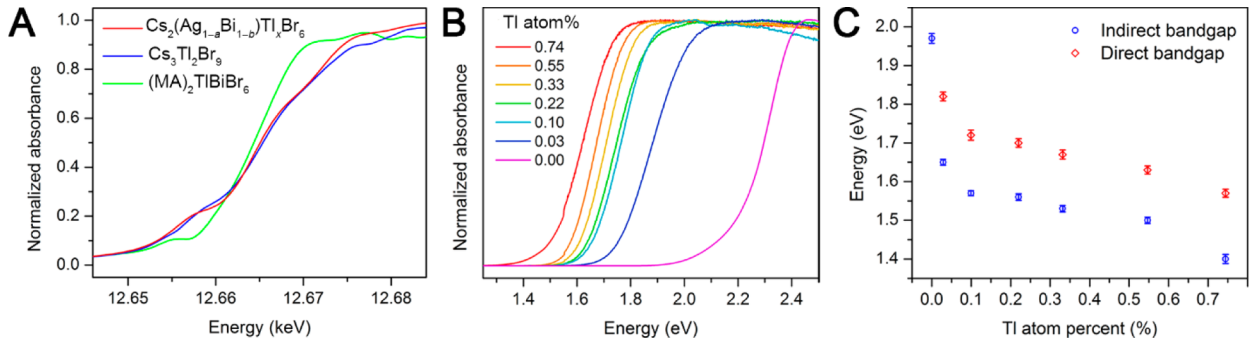

Figure 3. (A) X-ray near edge absorption structure (XANES) spectrum of $Cs_2(Ag_{1-a}Bi_{1-b})Tl_xBr_6$ (**1d**; $x = 0.075$) and spectra of Tl^+ and Tl^{3+} standards. (B) Absorbance spectra of **1d**. (C) Apparent bandgaps of **1d** extracted by linear fits to α^2 vs E (direct gap) and $\alpha^{1/2}$ vs E plots (indirect gap). Error bars represent the mean standard error.

0.075) resulting in 0.03−0.75 at. % Tl (Figure S1A and Table S1). Single-crystal X-ray diffraction (SC-XRD) showed **1d**'s structure to be nearly identical to that of **1** (Table S2). X-ray photoelectron spectroscopy (XPS) on **1d** crystals revealed diagnostic Tl 4f signals (Figure S2A) and sputtering experiments confirmed a uniform Tl distribution (Figure S2B). Thallium incorporation also red-shifts the broad band at 340 cm^{-1} in **1**'s Raman spectrum to 326 cm^{-1}, while a new band appears at 160 cm^{-1} (Figure S1B). Notably, **2**'s spectrum has a similar band at 163 cm^{-1}. To determine the Tl oxidation state, we measured the X-ray absorption near-edge structure (XANES) of **1d** (x = 0.075) at the Tl-L3 edge (Figure 3A). Although Tl^{3+} compounds display a distinctive XANES spectrum with three inflection points on the rising edge, Tl^+ compounds display only one.[8] Interestingly, the XANES spectrum of **1d** matches that for a Tl^{3+} compound with no indication of Tl^+.

We then calculated the energy gain/loss due to Tl substitution, $\Delta E = E^{doped} - E^{undoped}$, at both Ag^+ and Bi^{3+} sites using DFT within the generalized gradient approximation of Perdew, Burke, and Ernzerhof (PBE) as implemented in the VASP code.[9] We treat spin−orbit coupling (SOC) effects self-consistently (see Supporting Information). For **1d**; x = 0.25, substitution of Tl^{3+} for Bi^{3+} is thermodynamically uphill (ΔE = 0.7 eV). In contrast, substitution of Tl^+ for Ag^+ is energetically favorable (ΔE = −0.05 eV). For **1d**; x = 0.06, however, the energy difference between Tl substitution for Bi^{3+} and Ag^+ decreases significantly with $\Delta E(Bi^{3+})$ = 0.1 eV and $\Delta E(Ag^+)$ = −0.01 eV.

Noting that Tl^{3+} substitution for Bi^{3+} is less favored at higher x, we examined whether Tl^+/Ag^+ substitution occurs in the concentrated Tl regime by alloying Ag into the Tl−Bi perovskite: **2**. Synthesizing **2** in the presence of Ag^+ affords $(MA)_2(Tl_{1-a}Bi_{1-b})Ag_xBr_6$ (**2d**). Refining SC-XRD data for **2d** with full Tl occupancy shows substantial missing electron density at the Tl site (Figure S3). We modeled partial Ag substitution for Tl using 4 data sets collected at different X-ray wavelengths. From this analysis, we found ca. 20% Ag occupancy at the Tl site and a large improvement in refinement statistics (see Supporting Information), supporting the formula $(MA)_2(Tl_{0.8}Ag_{0.2})BiBr_6$. The presence of Ag in **2d** was further confirmed using XPS (Figure S2C), corroborating a Ag/Tl mixed site in **2d**. Our combined XANES, DFT, and SC-XRD results suggest that Tl can substitute at either Ag or Bi sites, and in the dilute alloying regime of **1d** substitution for Bi is dominant. The larger lattice in **2** may also more easily accommodate the larger Tl^+, whereas the smaller lattice in **1** is better suited for Tl^{3+} substitution.

DOI: 10.1021/jacs.7b01629
J. Am. Chem. Soc. 2017, 139, 5015−5018

To examine the optical effects of Tl alloying, reflectance spectra of **1** and **1d** were converted to pseudoabsorbance spectra using the Kubelka–Munk transformation[10] and bandgaps were extrapolated from α^r vs photon energy (E) plots (r = 0.5 and 2 for indirect and direct gaps, respectively; α = pseudoabsorption coefficient; Figures 3B,C, and S4). For **1**, these data corroborate the indirect bandgap previously reported.[4,5] For **1d**; x = 0.075, the data support either a direct gap of 1.6 eV or an indirect gap of 1.4 eV (see Supporting Information). The bandgap energy drops sharply from 1.95 eV in **1** (indirect) to 1.72 eV (direct) or 1.57 (indirect) in **1d**; x = 0.010. At x > 0.010, the gap decreases more slowly and reaches 1.40 eV (indirect) or 1.57 eV (direct) at the highest alloying level of x = 0.075. Interestingly, the bandgaps that arise from Tl alloying are much lower than those observed for undoped **1** (1.95 eV) or for the fully Tl-substituted **2** (2.16 eV). Notably, dilute Tl alloying brings **1**'s bandgap within the ideal range for a single-junction photovoltaic absorber.

Dopants can form recombination trap states that decrease carrier lifetime. We therefore performed time-resolved microwave photoconductivity (TRMC) measurements,[11] to directly probe free-carrier lifetime. Although carrier lifetime decreases upon alloying, **1d** exhibits long-lived carriers (with microsecond lifetime; Figure S5), suggesting that carriers can be efficiently extracted in a solar cell. Similar TRMC measurements on $(MA)PbI_3$ crystals revealed a carrier lifetime of ca. 15 μs.[12] A detailed analysis of our TRMC measurements will be reported separately. Our results show that **1d** is competitive with $(MA)PbI_3$ with respect to two key indicators for an efficient absorber: bandgap energy and carrier lifetime.

We performed DFT calculations to determine the evolution of **1d**'s electronic structure with Tl alloying, considering both Ag^+ and Bi^{3+} substitution. Figure 2c shows **1**'s band structure calculated with DFT-PBE+SOC (see Supporting Information) with the conduction bands rigidly shifted to reproduce the experimental bandgap. The CBM of **1** has Bi p character at Γ and Bi p–Ag s character at L because completely symmetric Ag s–Bi p hybridization is forbidden at Γ, but allowed at L. The calculated indirect (direct) bandgap is 1.09 eV (1.30 eV) underestimating experiment by ~0.9 eV, as expected from DFT-PBE and similar to the trends reported for $(MA)PbI_3$.[13] To obtain quantitative optical gaps, a more advanced treatment of exchange and correlation effects, including electron–hole interactions, is required. However, we expect that computed trends in bandgaps and relative energy differences between direct and indirect gaps will be captured reliably by DFT-PBE+SOC, at significantly less computational expense for these complex systems. We then constructed **1d** unit cells with 80, 160, and 320 atoms, where in each case substitution of one B-site atom with Tl corresponds to x = 0.13, x = 0.06, and x = 0.03, respectively. Keeping the lattice parameters fixed to those from experiment, we optimize all internal coordinates without symmetry constraints using DFT-PBE, and subsequently calculate the band structure along high-symmetry directions including spin–orbit interactions self-consistently. At x = 0.06, Tl^+ substitution for Ag^+ results in a direct gap at Γ and a bandgap reduction of ca. 0.1 eV (Figure 4A). Substitution of Tl^{3+} for Bi^{3+} shows a significantly larger bandgap reduction of ca. 0.8 eV, although the transition remains indirect (Figure 4B). Carrier effective masses for **1d**; x = 0.06 and for **1** are shown in Table S6; higher alloying levels may further increase band dispersion. Calculations for other x values are shown in Figures S6 and S7. We also constructed a **1d** unit cell with 320 atoms in which we substituted Tl^+ and Tl^{3+} at both Ag^+ and Bi^{3+} sites (**1d**; a = 0.03 and b = 0.03). This leads to a bandgap reduction of ca. 0.6 eV and an indirect bandgap only ca. 0.1 eV smaller than the direct transition at Γ (Figure S8). Calculations for only Tl^{3+} substitution and for mixed Tl^+/Tl^{3+} substitution both agree well with our optical data.

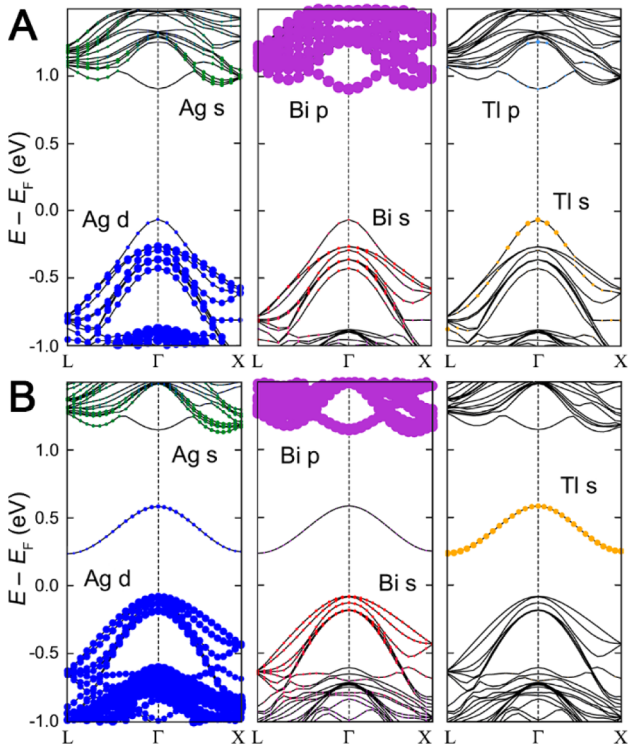

Figure 4. Band structures of $Cs_2(Ag_{1-a}Bi_{1-b})Tl_xBr_6$ (**1d**; x = 0.06) for (A) substitution of Tl^+ for Ag^+ and (B) substitution of Tl^{3+} for Bi^{3+}. Metal orbital characters of the bands are shown in color.

Consolidating our experimental and theoretical results we offer a model to explain the possible changes in **1**'s electronic structure upon dilute Tl alloying. Initial introduction of Tl^+ produces defect levels derived from Tl $6s^2$ and $6p^0$ orbitals, whereas introduction of Tl^{3+} affords defect levels stemming from Tl $5d^{10}$ and $6s^0$ orbitals. At low doping levels, this results in localized perturbations in the periodic lattice potential extending around the Tl impurity. As the Tl concentration increases, the average distance between Tl impurities rapidly diminishes. For example, at 0.1 at. % Tl (~10^{19} atoms/cm^3) the average distance between Tl atoms is 3.3 nm or ca. 3 unit cells and the localized impurity states interact with each other and the host lattice to modify the band edges. For Tl^{3+} substitution at Bi^{3+}, the average energy of the empty Tl s states is below **1**'s CBM, resulting in a new band that reduces the bandgap. This new band has Tl s and Ag d character and is consequently similar to the highest VB of **1**, placing the CBM at L. Comparable bandgap narrowing has been observed for isovalent alloying of $GaAs_{1-x}N_x$[14] and $GaN_{1-x}Sb_x$.[15]

Considering Tl^+ substitution at Ag^+, the average energy of the filled Tl s states is above **1**'s VBM, enabling a slight bandgap reduction. Additionally, Tl^+ substitution for Ag^+ introduces Tl p states at Γ that hybridize with Br p and Bi p orbitals, lowering the energy of the CBM at Γ and generating a direct gap. (Figure S6B). For equal substitution at both Ag and Bi sites, the CBM is dominated by the lower-energy Tl^{3+}-derived s orbitals instead of the higher-energy Tl^+-derived p orbitals, which maintains the indirect bandgap.

DOI: 10.1021/jacs.7b01629
J. Am. Chem. Soc. 2017, 139, 5015–5018

Solid **1d** retains the stability displayed by **1**,[4] with no changes in its PXRD patterns upon exposure to 0.75 sun at ca. 60 °C under N_2 for 30 days, 90 °C in air for 5 days, and 55% relative humidity under N_2 for 30 days (Figure S9). Although Tl^+ is ca. 10 times more toxic than Pb^{2+}, complete replacement of Pb^{2+} with a fraction of Tl^+ results in an overall decrease in toxicity. Although semiconductor doping has played a central role in the photovoltaics industry, the effects of doping $APbX_3$ perovskites are only just being explored. The most pronounced effects have been seen in heavily alloyed $(MA)Pb_{1-x}Sn_xI_3$, where x = 0.25−0.5 afforded a 0.4 eV bandgap reduction,[16] and in doped $(MA)Pb_{1-x}Bi_xBr_3$ where x = 0.03 resulted in a 0.3 eV bandgap decrease.[17]

Here we demonstrate that halide double perovskites have rich substitutional chemistry, which can engender dramatic changes to their photophysical properties. In the concentrated Tl regime, Tl^+/Ag^+ site mixing occurs readily, as in $(MA)_2(Tl_{1-a}Bi_{1-b})$-Ag_xBr_6 (**2d**; x = 0.2). At lower Tl levels, Tl^{3+} appears to predominantly substitute for Bi^{3+} as in $Cs_2(Ag_{1-a}Bi_{1-b})Tl_xBr_6$ (**1d**; x = 0.075). Optical spectra reveal that the latter results in a bandgap decrease of ca. 0.5 eV. Calculations show that dilute Tl^+ alloying (x = 0.06) at Ag^+ sites in **1d** results in a 0.1 eV bandgap reduction and conversion to a direct gap, whereas Tl^{3+} substitution at Bi^{3+} sites affords a 0.8 eV reduction in bandgap, with the gap remaining indirect. Predominant substitution of Tl^{3+} for Bi^{3+} in **1d**, where atmospheric oxygen mediates the oxidation of Tl^+ to Tl^{3+}, is most consistent with our experimental results.

The optoelectronic properties of **1d** motivate the continued exploration of impurity alloying in double perovskites. Importantly, by describing how dopant orbitals at low concentrations selectively modify **1**'s band edges, we provide guidelines for identifying other dopants that can afford large bandgap reductions and direct-gap transitions in environmentally benign double perovskites.

■ ASSOCIATED CONTENT

Supporting Information

The Supporting Information is available free of charge on the ACS Publications website at DOI: 10.1021/jacs.7b01629.

Experimental details, crystallographic data, and spectra (PDF)
Data for $AgBiBr_6Cs_2$ (CIF)
Data for $C_2H_{12}Ag_{0.2}BiBr_6N_2Tl_{0.8}$ (CIF)
Data for $C_2H_{12}BiBr_6N_2Tl$ (CIF)

■ AUTHOR INFORMATION

Corresponding Authors

*hemamala@stanford.edu
*jbneaton@lbl.gov

ORCID

Michael F. Toney: 0000-0002-7513-1166
Hemamala I. Karunadasa: 0000-0003-4949-8068

Notes

The authors declare no competing financial interest.

■ ACKNOWLEDGMENTS

We thank Adam Jaffe, Dr. Yu Lin, Dr. Simon Teat, Matthew Latimer, Erik Nelson, and Jung-Hoon Lee for experimental assistance. SC-XRD experiments used beamline 11.3.1 at the Advanced Light Source (ALS). XANES measurements used beamline 2-2 at the Stanford Synchrotron Radiation Lightsource (SSRL). A.H.S. is supported by a Stanford Graduate Fellowship. This work was funded by the SLAC National Accelerator Laboratory and the Alfred P. Sloan Fellowship. J.B.N. and L.L. were supported by the U.S. Department of Energy, Office of Science, Office of Basic Energy Sciences (DOE, BES), Materials Sciences and Engineering Division (DE-AC02-05CH11231). L.L. is supported by the Feodor-Lynen program of the Alexander von Humboldt foundation. Work at the Molecular Foundry, ALS, and SSRL was supported by the DOE, BES (DE-AC02-05CH11231 for the Molecular Foundry and ALS, and DE-AC02-76SF00515 for SSRL). Work by D.B. and T.J.S. was funded by the Partnership Program of the Materials Innovation Institute M2i and the Foundation of Fundamental Research on Matter, Netherlands Organization for Scientific Research (F71.4.15562a). A.G.-P. is supported by an NSF GRFP (DGE-1147470).

■ REFERENCES

(1) (a) Kojima, A.; Teshima, K.; Shirai, Y.; Miyasaka, T. *J. Am. Chem. Soc.* **2009**, *131*, 6050. (b) Zhang, W.; Eperon, G. E.; Snaith, H. J. *Nat. Energy* **2016**, *1*, 16048.

(2) (a) Needleman, H. *Annu. Rev. Med.* **2004**, *55*, 209. (b) Babayigit, A.; Ethirajan, A.; Muller, M.; Conings, B. *Nat. Mater.* **2016**, *15*, 247.

(3) Slavney, A. H.; Smaha, R. W.; Smith, I. C.; Jaffe, A.; Umeyama, D.; Karunadasa, H. I. *Inorg. Chem.* **2017**, *56*, 46.

(4) Slavney, A. H.; Hu, T.; Lindenberg, A. M.; Karunadasa, H. I. *J. Am. Chem. Soc.* **2016**, *138*, 2138.

(5) McClure, E. T.; Ball, M. R.; Windl, W.; Woodward, P. M. *Chem. Mater.* **2016**, *28*, 1348.

(6) (a) Volonakis, G.; Filip, M. R.; Haghighirad, A. A.; Sakai, N.; Wenger, B.; Snaith, H. J.; Giustino, F. *J. Phys. Chem. Lett.* **2016**, *7*, 1254. (b) Wei, F.; Deng, Z.; Sun, S.; Xie, F.; Kieslich, G.; Evans, D. M.; Carpenter, M. A.; Bristowe, P. D.; Cheetham, A. K. *Mater. Horiz.* **2016**, *3*, 328. (c) Deng, Z.; Wei, F.; Sun, S.; Kieslich, G.; Cheetham, A. K.; Bristowe, P. *J. Mater. Chem. A* **2016**, *4*, 12025. (d) Volonakis, G.; Haghighirad, A. A.; Milot, R. L.; Sio, W. H.; Filip, M. R.; Wenger, B.; Johnston, M. B.; Herz, L. M.; Snaith, H. J.; Giustino, F. *J. Phys. Chem. Lett.* **2017**, *8*, 772.

(7) Filippetti, A.; Mattoni, A. *Phys. Rev. B: Condens. Matter Mater. Phys.* **2014**, *89*, 125203.

(8) Arvind, A.; Vishnoi, A. N. *Phys. Scr.* **2005**, *2005*, 534.

(9) (a) Perdew, J. P.; Burke, K.; Ernzerhof, M. *Phys. Rev. Lett.* **1996**, *77*, 3865. (b) Kresse, G.; Furthmüller, J. *Phys. Rev. B: Condens. Matter Mater. Phys.* **1996**, *54*, 11169.

(10) Kubelka, P.; Munk, F. *Z. Technol. Phys.* **1931**, *12*, 593.

(11) Savenije, T. J.; Ferguson, A. J.; Kopidakis, N.; Rumbles, G. *J. Phys. Chem. C* **2013**, *117*, 24085.

(12) Bi, Y.; Hutter, E. M.; Fang, Y.; Dong, Q.; Huang, J.; Savenije, T. J. *J. Phys. Chem. Lett.* **2016**, *7*, 923.

(13) Brivio, F.; Butler, K. T.; Walsh, A.; van Schilfgaarde, M. *Phys. Rev. B: Condens. Matter Mater. Phys.* **2014**, *89*, 155204.

(14) Weyers, M.; Sato, M.; Ando, H. *Jpn. J. Appl. Phys.* **1992**, *31*, L853.

(15) Sunkara, S.; Vendra, V. K.; Jasinski, J. B.; Deutsch, T.; Andriotis, A. N.; Rajan, K.; Menon, M.; Sunkara, M. *Adv. Mater.* **2014**, *26*, 2878.

(16) Hao, F.; Stoumpos, C. C.; Chang, R. P. H.; Kanatzidis, M. G. *J. Am. Chem. Soc.* **2014**, *136*, 8094.

(17) Abdelhady, A. L.; Saidaminov, M. I.; Murali, B.; Adinolfi, V.; Voznyy, O.; Katsiev, K.; Alarousu, E.; Comin, R.; Dursun, I.; Sinatra, L.; Sargent, E. H.; Mohammed, O. F.; Bakr, O. M. *J. Phys. Chem. Lett.* **2016**, *7*, 295.

DOI: 10.1021/jacs.7b01629
J. Am. Chem. Soc. 2017, 139, 5015−5018